"Frozen" Block Copolymer Nanomembranes with Light-Driven Proton Pumping Performance

Liangju Kuang,[†] Donald A. Fernandes,[‡] Matthew O'Halloran,[‡] Wan Zheng,[†] Yunjiang Jiang,[†] Vladimir Ladizhansky,[‡] Leonid S. Brown,[‡,*] and Hongjun Liang[†,*]

[†]Department of Metallurgical and Materials Engineering, Colorado School of Mines, Golden, Colorado 80401, United States, and [‡]Department of Physics, University of Guelph, Guelph, Ontario, Canada N1G 2W1

ABSTRACT

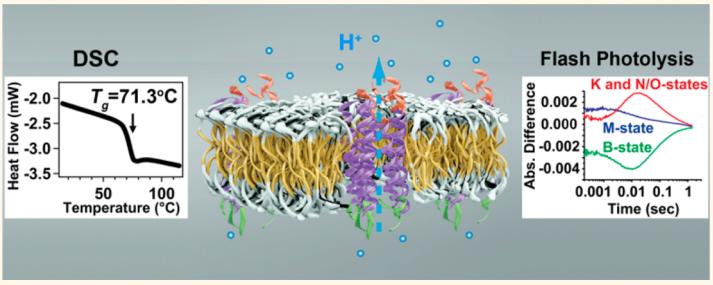

Cellular membranes are natural nanoengineering devices, where matter transport, information processing, and energy conversion across the nanoscale boundaries are mediated by membrane proteins (MPs). Despite the great potential of MPs for nanotechnologies, their broad utility in engineered systems is limited by the fluidic and often labile nature of MP-supporting membranes. Little is known on how to direct spontaneous reconstitution of MPs into robust synthetic nanomembranes or how to tune MP functions through rational design of these membranes. Here we report that proteorhodopsin (PR), a light-driven proton pump, can be spontaneously reconstituted into "frozen" (*i.e.*, glassy state) amphiphilic block copolymer membranes *via* a charge-interaction-directed reconstitution mechanism. We show that PR is not enslaved by a fluidic or lipid-based membrane environment. Rather, well-defined block copolymer nanomembranes, with their tunable membrane moduli, act as allosteric regulators to support the structural integrity and function of PR. Versatile membrane designs exist to modulate the conformational energetics of reconstituted MPs, therefore optimizing proteomembrane stability and performance in synthetic systems.

KEYWORDS: membrane protein · polymersome · proton pump · nanomembrane · solar energy conversion · charge-interaction-directed reconstitution · self-assembly · directed assembly

Integral membrane proteins (MPs), which are characterized by a hydrophobic membrane-spanning domain and hydrophilic extramembrane regions, mediate diverse recognition and transport functions across the membrane boundaries.[1] Adapting artificial systems to support MP functions may help understand, predict, and ultimately control matter and energy at the nanoscale; this is particularly enticing in the postgenomic era as recombinant or cell-free expression of these MPs in sizable quantities became feasible.[2,3] Since Mueller's pioneering work on reconstituting a cell membrane structure,[4] great progress has been made on MP reconstitution into different forms of lipid bilayers[5−8] and fluidic polymersome membranes.[9−13] However, the labile nature of these membranes limits their use under a broad range of engineered conditions. Strengthening methods such as cross-linking,[14] chemical bonding with a supporting substrate,[15] and encapsulation[16,17] have been used to improve the stability of membranes, but it is desirable to develop synthetic nanomembranes that are sufficiently strong by themselves to support MPs without compromising the protein's structural integrity and functions.

Fluidity is often regarded essential for biomembranes,[18,19] but stability is highly valued in engineered systems.[16] Recent studies

* Address correspondence to lebrown@uoguelph.ca; hjliang@mines.edu.

Received for review September 30, 2013 and accepted December 22, 2013.

Published online December 23, 2013
10.1021/nn4059852

revealed that native MP-supporting biomembranes are actually more mosaic than fluid,[20,21] a condition that is hard to reproduce in artificial systems when lipids are used alone. How to design MP-supporting membranes that balance a dichotomy between fluidity and stability is a critical but not well understood issue. The reductionist view of biology assumes MPs and biomembranes must have coevolved, such that lipids become indispensable components. The important roles of specific endogenous lipids in MP functions have been demonstrated in many studies,[22−25] while there is also compelling evidence suggesting MP−lipid partnership is not exclusive, and the role of lipids may be related to their contribution to the bulk physical properties of MP-supporting membranes, such as curvature, lateral pressure profile, and thickness.[26−30] These seemingly contradictory recognitions may be reconciled by the observation of tightly bound lipids on MPs, distinct from "solvent" lipids that are further apart.[31−34] Unlike "solvent" lipids that collectively define bulk membrane properties, MP-bound lipids may supplement specific interactions critical for MPs' structural integrity and functions. By choosing detergents that do not disrupt this specific pairing, it is possible to stably extract many MPs from their native environment,[35] therefore creating a family of biologically derived nanomaterials (*i.e.*, MPs) to be explored in synthetic systems. Pioneering studies by Meier *et al.*[9] and others[10−13] have shown that detergent-solubilized MPs can be functionally reconstituted into fluidic polymersome membranes, primarily polydimethylsiloxane (PDMS)-based membranes with a PDMS block size far smaller than its entanglement molecular weight. What remains poorly understood though is how to direct spontaneous reconstitution of MPs into robust synthetic nanomembranes and how to tune MP functions through rational design of these membranes.

The limited choice of MP-supporting membranes may reflect the working mechanism of conventional MP reconstitution methods: they rely critically on detergent solubilization or mechanical agitation to destabilize membranes followed by delicate and time-consuming external means to remove detergent; this eventually results in a transition from MP−detergent−lipid coassembled states to proteomembranes.[36−40] Using proteorhodopsin (PR), a light-driven proton pump with a common seven transmembrane (7TM) architecture of G protein-coupled receptors (GPCRs) as an example,[41,42] we revealed a charge-interaction-directed reconstitution (CIDR) mechanism that induces formation of 2-D or 3-D polarized proteolipid membrane arrays spontaneously without detergent removal.[43,44] We further showed that CIDR can be applied to induce spontaneous reconstitution of PR[45] and bacterial photosynthetic reaction center (an MP that has three subunits and is ∼4× larger than PR)[46] into polybutadiene (PBD)-based block copolymer membranes even when PBD is in an entangled state with greatly enhanced stability. Here, we report that spontaneous reconstitution of PR into "frozen" polymersome membranes, which have unsurpassed stability as MP-supporting matrices, is achieved *via* the CIDR mechanism. The broad utility of CIDR enables systematic study of matrix-dependent MP functions in a wide range of synthetic nanomembranes; this aspect has not been examined with conventional MP reconstitution methods. We show here that the PR-supporting polymersome membranes act as allosteric regulators: increasing membrane-forming block size and rigidity gives rise to increasingly restricted light-induced conformational dynamics of PR. Counterintuitively, the kinetics of PR-mediated proton-pumping across "frozen" polymer membranes is tunable to rival that in lipid bilayers, underscoring the possibility to balance local chain-motion freedom and bulk-state membrane stability at the nanoscale.

RESULTS AND DISCUSSION

We expressed PR (*BAC31A08*) in *E. coli* and extracted and purified the MP with *n*-dodecyl-β-D-maltoside (DDM). The isoelectric point of DDM-solubilized PR was determined as 4.5.[44] Using controlled/living free radical polymerization methods (Supporting Information, SI),[47,48] we synthesized a series of well-defined and cationically charged amphiphilic block copolymers, polystyrene-*b*-poly(4-vinyl-*N*-methylpyridine iodide)$_2$ (PS-*b*-P4MVP$_2$), which have a "frozen" membrane-forming PS block of tunable size (SI). For example, to prepare the block copolymer *via* reversible addition−fragmentation chain-transfer (RAFT) polymerization, we first prepared a bifunctional chain transfer agent (bi-DATC) by coupling *S*-1-dodecyl-*S*′-(α,α′-dimethyl-α″-acetic acid) trithiocarbonate (DATC)[49] with ethylene glycol (Figure S1). The bi-DATC was then used to prepare PS blocks with near-unity polydisperse indices (PDIs), as shown by gel permeation chromatography (GPC), differential scanning calorimetry (DSC), and ^{1}H nuclear magnetic resonance (^{1}H NMR) studies (Figure S2). We then used the PS blocks as bifunctional macro chain transfer agents to add poly(4-vinylpyridine) (P4VP) blocks on both ends. We finally converted the PS-*b*-P4VP$_2$ block copolymers to their cationic forms by a quaternarization reaction after cleaving the trithiocarbonate moieties.[45] We also prepared PS-*b*-P4MVP$_2$ *via* atom-transfer radical polymerization (ATRP) to address potential instability of ester bonds introduced in RAFT polymerization. A combination of characterization methods was used to characterize the polymer products at each synthesis step, and the results were mutually consistent (SI). We confirmed that PS-*b*-P4MVP$_2$ prepared by both polymerization approaches behaved in the same way: they self-assembled into polymersomes in water, and these polymersomes directed spontaneous and functional reconstitution of PR, *vide infra*.

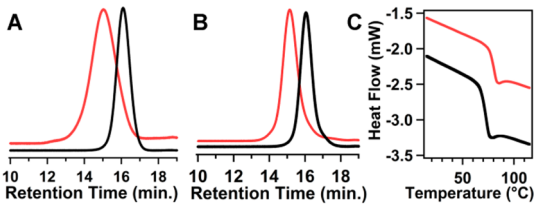

Figure 1. Well-defined amphiphilic triblock copolymers PS-*b*-(P4MVP)$_2$ prepared *via* controlled/living free radical polymerization methods. (A) GPC of PS$_{26}$ block (black trace, M_n/PDI: 2600 Da/1.17) and PS$_{26}$-*b*-(P4VP$_{21}$)$_2$ triblock copolymer (red trace, M_n/PDI: 7300 Da/1.22; shifted upward for clarity). (B) GPC of PS$_{42}$ block (black trace, M_n/PDI: 4200 Da/1.18) and PS$_{42}$-*b*-(P4VP$_{29}$)$_2$ triblock copolymer (red trace, M_n/PDI: 10 500 Da/1.10; shifted upward for clarity). (C) DSC of PS$_{26}$ (black trace) and PS$_{42}$ blocks (red trace) reveals their T_g at 71.3 and 79.6 °C, respectively.

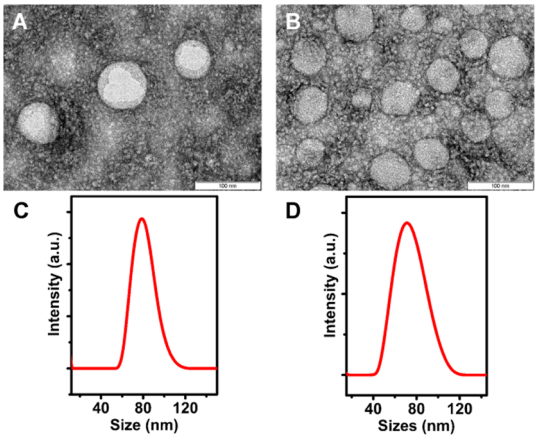

Figure 2. The amphiphilic triblock copolymers PS-*b*-(P4MVP)$_2$ self-assemble in water into polymersomes. The polymersome morphology of PS$_{26}$-*b*-(P4MVP$_{21}$)$_2$ (A) and PS$_{42}$-*b*-(P4MVP$_{29}$)$_2$ (B) is clearly revealed by TEM (scale bar: 100 nm; stained with 1% UAc), and their respective size distribution is confirmed by DLS (C, D).

We focus our discussion on two representative block copolymers that have different membrane-forming block sizes, PS$_{26}$-*b*-(P4MVP$_{21}$)$_2$ and PS$_{42}$-*b*-(P4MVP$_{29}$)$_2$. Their well-defined structures were confirmed by GPC (Figure 1A, B) and ^{1}H NMR studies (Figure S3). Both membrane-forming PS blocks are in a "frozen" state at room temperature, as expected from their glass transition temperature (T_g) at 71.3 and 79.6 °C, respectively (Figure 1C).

The amphiphilic triblock copolymers self-assemble in water into polymersomes, most of which have a diameter of ~80 ± 20 nm, as revealed by transmission electron microscopy (TEM) and dynamic light scattering (DLS) (Figure 2). It has been shown that the membrane-forming blocks in polymersomes assume a theta-state.[50,51] We confirmed that the theta-state PS in both polymersomes remains "frozen". For example, the T_g of PS$_{26}$-*b*-(P4MVP$_{21}$)$_2$ polymersomes in aqueous solution was measured as 66.3 °C (Figure 3C), which matches closely that of the membrane-forming PS$_{26}$ block measured in its solid state (*i.e.*, 71.3 °C, Figure 1C).

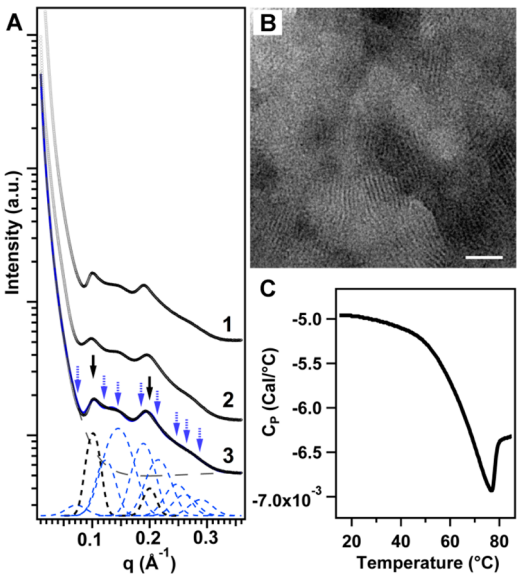

Figure 3. CIDR induces spontaneous PR reconstitution into "frozen" PS-*b*-(P4MVP)$_2$ membranes. (A) Synchrotron SAXS of proteopolymer complexes (trace 1: PR and PS$_{26}$-*b*-(P4MVP$_{21}$)$_2$; trace 2: PR and PS$_{38}$-*b*-(P4MVP$_{21}$)$_2$; trace 3: PR and PS$_{42}$-*b*-(P4MVP$_{29}$)$_2$). The SAXS spectra are characterized by two strong harmonics (marked by black solid arrows) and a series of diffusive scatterings that are clearly discernible albeit weak (marked by blue dotted arrows). As an example shown for trace 3, the SAXS spectra are fitted to reveal a background scattering (dashed line), a multilamellar proteomembrane structure (black dotted peaks, q_{001} = 0.101 Å^{-1}) that agrees well with TEM observation (panel B), and a 2-D hexagonally packed PR lattice in individual membranes (blue dotted peaks centered at 0.072, 0.124, 0.145, 0.189, 0.215, 0.247, and 0.26 Å^{-1}, corresponding to q_{10}, q_{11}, q_{20}, q_{12}, q_{30}, q_{22}, and q_{13}, respectively; note that the first peak at q_{10} is shadowed by strong scattering in the vicinity of the beam stop and appears weak). The summation (solid blue trace) of all scattering contributions overlaps nicely with the scattering data (○). (B) TEM of proteopolymer complexes (PR and PS$_{42}$-*b*-(P4MVP$_{29}$)$_2$, stained with 1% UAc) confirms the multilamellar proteopolymer membrane structure ($d \approx$ 6.0 nm). Scale bar: 50 nm. (C) DSC confirms that the polymersome membrane (PS$_{26}$-*b*-(P4MVP$_{21}$)$_2$) is "frozen" (T_g = 66.3 °C) in solution.

We prepared a series of proteopolymer complexes composed of PR and well-defined "frozen" PS-*b*-(P4MVP)$_2$ membranes with systematically varied PS block sizes: PS$_{26}$-*b*-(P4MVP$_{21}$)$_2$, PS$_{38}$-*b*-(P4MVP$_{21}$)$_2$ (Figure S4), and PS$_{42}$-*b*-(P4MVP$_{29}$)$_2$. Their spontaneous reconstitution occurs *via* the CIDR mechanism at pH 7.4, where both extramembrane regions of PR are anionically and asymmetrically charged.[45] The oppositely charged polymersomes and DDM-solubilized PR spontaneously coassembled to form condensed proteopolymer complexes without detergent removal, and the settled proteopolymer membranes can be easily separated from the rest of the supernatant and redispersed in a different buffer if needed, for structural and functional assays.

TEM of all three proteopolymer complexes revealed a striking morphological transition from spherical polymersomes to stacked proteopolymer membrane arrays, with a similar lamellar periodicity of ~6.0 nm

(Figure 3B). It has been shown that the thickness (d) of theta-state polymersome membranes can be estimated from the mean-square end-to-end distance ($\langle R^2 \rangle$) of the membrane-forming blocks, yielding identical results to that measured by cryo-TEM.[45] Given Flory's characteristic ratio of PS ($C_\infty = 9.5$),[52] the PS_{26}, PS_{38}, and PS_{42} membrane thickness was estimated using $d = (\langle R^2 \rangle)^{1/2} = (C_\infty n l^2)^{1/2}$ (where n and l represents the number and length of C−C bonds) to be 3.4, 4.1, and 4.4 nm, respectively. Since DDM-solubilized PR (*i.e.*, PR-DDM micelles) has an overall size of 16 ± 3 nm at pH = 7.4,[44] the observed lamellar periodicity of 6.0 nm cannot physically fit any forms of random flocculation between polymersome membranes and DDM-solubilized PR, but is sufficient to fit a transmembrane dimension of PR (~5.5 nm), suggesting that the PR-associated DDM micelles are decorticated during the CIDR process.[45] A reconstituted state of PR was also confirmed by the same lamellar periodicity observed for all proteopolymer complexes, agreeing with simulations that polymersome membranes are able to accommodate the dimension of reconstituted MPs *via* hydrophobic matching.[53,54]

Synchrotron small-angle X-ray scattering (SAXS) studies further confirmed the successful CIDR of PR in "frozen" polymersome membranes (Figure 3A). Despite the difference in polymersome membrane thickness, SAXS spectra of all proteopolymer complexes are nearly identical: there are two strong harmonics (marked by black solid arrows) and a series of diffusive scatterings that are clearly discernible albeit weak (marked by blue dotted arrows). The two strong harmonics are attributed to the multilamellar proteopolymer membrane structure without ambiguity, as its lattice spacing, judged by its first harmonics (q_{001} = 0.101 Å^{-1}), agrees nicely with the well-ordered stacking-layer structure observed in TEM (Figure 3B). The shape of these two strong harmonics and their relative positions further reveal the coexistence of other structural features. For instance, additional shoulder peaks are clearly discernible on the right side of the first harmonic peak and both sides of the second harmonic peak, as their contributions render both peaks asymmetrically shaped, and slightly shift the apparent center of the second harmonics from 0.202 Å^{-1} (as expected) to 0.194 Å^{-1}. These fine scattering features can be attributed only to in-membrane protein correlations.

To better understand the structure of these proteopolymer complexes, we fit the SAXS data with different proteopolymer membrane structural models using the nonlinear least-squares method. Our data analysis revealed that a 2-D hexagonally packed PR lattice in individual proteomembrane layers is the most plausible choice to account for all the fine scattering features: a full set of the first seven characteristic scatterings of the 2-D PR hexagonal lattice from q_{10} to q_{13} (blue dotted peaks, q_{10} = 0.072 Å^{-1}) shows up nicely (Figure 3A). These scattering peaks show consistent full width at half-maximum (0.04−0.045 Å^{-1}) and form factor, except for the first peak at q_{10}, which is shadowed by strong scattering in the vicinity of the beam stop and appears weak. This 2-D PR lattice has a lattice parameter (a = 101 Å) similar to that observed previously,[44,45,55] suggesting consistent PR packing arrangement within a supporting membrane. The diffusive nature of these correlations, however, suggests that the 2-D proteopolymer lattice is fairly imperfect, probably due to the "frozen" nature of PS chains that restricts PR reorganization to achieve highly ordered states. For instance, estimation using the Scherrer equation suggests that the coherent PR crystalline domain size is only ~30−40 nm, *i.e.*, spanning across ~3−4 PR hexagonal lattice units. Furthermore, since rhodopsins have a typical hydrophobic size of 3.5 nm or less,[32] considerable hydrophobic mismatch is expected when PR is reconstituted in PS_{42} membrane. Interestingly, SAXS confirmed that all proteopolymer membranes have identical lamellar periodicity, suggesting that the nanoscale polymersome membranes, even when "frozen", have sufficient conformational freedom to match the hydrophobic domain of reconstituted PR.

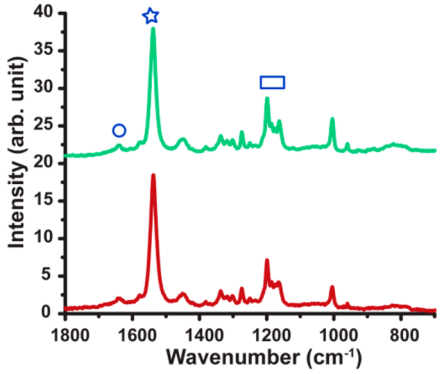

Figure 4. Raman spectra of PS_{42} proteopolymer complexes (green) and DMPC/DMPA proteoliposome complexes (red) reveal identical retinal vibrational peaks. The retinal fingerprint C−C stretches, ethylenic C═C stretch, and Schiff base C═N stretch are marked by a rectangle, star, and circle, respectively.

Using PR that was uniformly isotope labeled with ^{15}N and alternately labeled with ^{13}C by growing the protein on 2-^{13}C glycerol, we examined the structural integrity of reconstituted PR in "frozen" polymer membranes with Raman (Figure 4) and solid-state NMR (ssNMR) spectroscopy (Figure 5). We confirmed that the native-like PR structure is maintained even when reconstituted in a cationically charged and mismatched "frozen" PS_{42} membrane.

The retinal chromophore of PR, which is central to PR's light-driven proton-pumping performance, is positioned in a hydrophobic pocket *via* a Schiff base conjugation with a Lys231 side-chain on helix G.

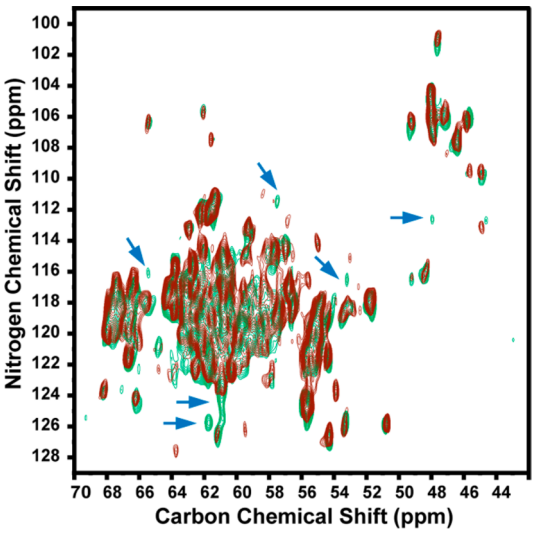

Figure 5. 2-D NCA ssNMR spectra of PS_{42} proteopolymer complexes (green) and DMPC/DMPA proteoliposome complexes (red). See text for details.

Any change of its local chemical environment, *e.g.*, alteration of PR tertiary structure, will be sensitively reflected in retinal Raman bands. We compared the Raman spectrum of ^{15}N,^{13}C-labeled PR reconstituted in "frozen" PS_{42}-*b*-$(P4MVP_{29})_2$ membranes (green trace, Figure 4) with that in a liposome system (red trace) recently used to determine PR secondary structure by ssNMR,[56,57] *i.e.*, a binary mixture of 1,2-dimyristoyl-*sn*-glycero-3-phosphocholine (DMPC) and 1,2-dimyristoyl-*sn*-glycero-3-phosphate (DMPA) (w/w = 9:1). We confirmed that PR reconstituted in both membranes has identical Raman spectra (Figure 4). For instance, the relative ratio and width of retinal fingerprint C−C stretches (1199/1186/1162 cm^{-1}, marked by a rectangle), ethylenic C═C stretch (1538 cm^{-1}, marked by a star), and Schiff base C═N stretch (1639 cm^{-1}, marked by a circle) are exactly the same, suggesting invariant chromophore−protein local interactions.

We also compared the 2-D ssNMR NCA spectra (*i.e*, correlations of spins of the backbone N and Cα atoms) of ^{13}C,^{15}N-labeled PR in both proteomembranes (Figure 5). Chemical shifts in NCA spectra are strongly dependent on backbone torsion angles[58] (*i.e.*, PR secondary structure), while the intensity of the peaks in PR depends on the protein dynamics.[57] The unprocessed (*i.e.*, measured without applying a window function prior to Fourier transform) carbon line widths of both spectra were found to be in the same range of 0.25−0.35 ppm, typical of structurally homogeneous samples. We observed close agreement between the cross-peak positions in the spectra of both proteomembranes, indicating similar PR secondary structure. A few extra peaks showing up in PS_{42} membranes (marked by arrows) may be attributed to some additional immobilized amino acids outside the transmembrane helices of PR, possibly due to a different hydrophilic−hydrophobic interface in the multilamellar proteopolymer membranes. To the best of our knowledge, this is the first example of an ssNMR study on MPs reconstituted in "frozen" proteopolymer membrane, a system that may open new opportunities for structural analysis of MPs by ssNMR methods.

PR reconstituted in "frozen" polymer membranes is confined within a fundamentally different supporting media as compared to lipid-based biomembranes. Very little is known on how MP functions are regulated by synthetic nanomembranes other than lipid bilayers. We applied time-resolved visible spectroscopy (*i.e.*, flash-photolysis) to quantitatively probe PR functionality. Flash-photolysis has been used extensively for the functional characterization of rhodopsins, including PR,[7,59−61] by monitoring their key photocycle steps and overall turnover kinetics. We used the most important wavelengths indicative of PR's normal proton pumping function: (1) 420 nm, M intermediate reporting on the deprotonation and reprotonation of the retinal Schiff base; (2) 600 nm, red-shifted K and N/O intermediates reporting on retinal isomerization as well as isomeric composition of the dark state; (3) 500 nm, bleaching of the dark parent state reporting on the overall photocycle turnover kinetics. The key indicators of native-like behavior of PR in proteopolymer membranes are the presence of the M intermediate at 420 nm, the absence of strong signals from the 13-*cis*-dark state at 600 nm (distinct from those of the red-shifted K and N/O intermediates), and relatively fast (hundreds of ms) photocycle turnover kinetics as measured at 500 and 600 nm.

Representative single-wavelength light-induced kinetics traces are shown in Figure 6. As the membrane-forming PS block size increases from PS_{26} (Figure 6A) to PS_{38} (Figure 6B), and to PS_{42} (Figure 6C), continuous deceleration of the PR photocycle was observed. To quantitatively compare the overall photocycle behavior, we applied global exponential fitting to all traces to extract the kinetic data.[63] The kinetic data from different proteomembranes (limited to statistically valid four-exponential fits) are summarized and compared in Table 1. Note that because the true photointermediates exist in equilibria, each of the apparent kinetic states is a mixture of two or more intermediates. As such, the same kinetic components can show up in the decay of different intermediates.[59,60]

Although the exact kinetic model of PR's photocycle is unknown so far, our phenomenological time constants derived from the kinetic traces tracking PR's key photocycle intermediates, as shown in Table 1, clearly demonstrate that PR's proton-pumping function is critically dependent on the physical properties of PR-supporting matrices: while structurally intact PR is reconstituted in all polymer membranes, its proton-pumping photocycles slow down as the membrane block size and rigidity increase. We reason that PR,

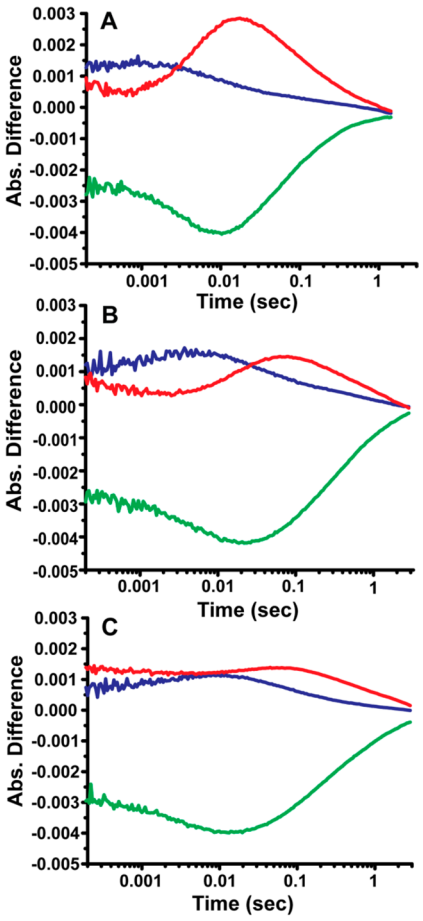

Figure 6. Kinetics of the proton-pumping photocycles of PR reconstituted in "frozen" polymersome membranes. The light-induced absorption difference changes reflecting the characteristic photocycle intermediate states of PR reconstituted in (A) PS_{26}-*b*-$(P4MVP_{21})_2$, (B) PS_{38}-*b*-$(P4MVP_{21})_2$, and (C) PS_{42}-*b*-$(P4MVP_{29})_2$ membranes are shown (red trace: K and N/O states, 600 nm; green: the parent dark state, 500 nm; and blue: M state, 420 nm).

TABLE 1. Photocycle Kinetics of PR Reconstituted in Different Membranes (pH = 9)

membrane	M rise	M decay	N/O decay
DDM-treated *E. coli* membr.[a]	12/120/800 μs	2/9.4 ms	9.4/35/230 ms
DMPC/DMPA (w/w = 9:1)[62]	?[b]/853 μs	3.6/29/241 ms	29/241 ms
PS_{26} membrane	?/613 μs	4.9/40/260 ms	40/260 ms
PS_{38} membrane	?/1.5 ms	14/74/649 ms	74/649 ms
PS_{42} membrane	?/2.8 ms	25/112/878 ms	112/878 ms

[a] Measured at pH = 9.5 (ref 59). [b] Unresolved due to strong Rayleigh scattering.

like many other MPs, need to perform conformational changes to function.[64] The energetics associated with these expansion and/or stretching modes are tuned by the physical properties of supporting membranes, such as compression (K_a) and bending moduli (K_c).[29,30,45] K_a is primarily related to the interfacial tension (γ), *i.e.*, $K_a \approx 4\gamma$,[65,66] and K_c can be modeled as $\sim\beta K_a d^x$,[67,68] where β is a constant reflecting membrane interdigitation or entanglement, d is membrane thickness, and x is a scaling factor depending strongly on membrane chain flexibility. By increasing "frozen" PS block sizes, we further reduce the membrane fluidity (*i.e.*, K_c ↑) and conformational freedom of the membrane-forming blocks (*i.e.*, *via* hydrophobic matching). Not surprisingly, we observed deceleration of all photocycle phases, indicating that a less fluidic, compressed polymer membrane impedes PR conformational changes in general. We note that the physics behind this allosteric regulation is independent of specific PR–membrane chemical interactions. Similar slowed-down photocycle kinetics was also observed when PR is confined in lipid nanodiscs.[7] Although it has been recognized that the physical properties of lipid bilayers play important roles in MP functions,[26−30] it is generally challenging to distinguish bulk effects from specific ones in lipid-based membranes.[24] Using non-lipid-based synthetic nanomembranes, we unambiguously demonstrate here that PR-supporting membranes act as allosteric regulators for its function.

Surprisingly, the photocycle kinetics of PR reconstituted in the "frozen" PS_{26} membranes approaches the reported numbers in DDM-treated, PR-containing *E. coli* membrane (Table 1).[59] This suggests that "frozen" polymer membranes, with their reduced fluidity and greatly enhanced stability, can still bear sufficient conformational freedom that rivals lipid-based biomembranes in supporting MP functions. We expect that versatile polymer membrane designs can be created to balance membrane fluidity and stability at the nanoscale. This modulates the conformational energetics of reconstituted MPs, hence optimizing proteomembrane stability and performance in synthetic systems.

CONCLUSION

In summary, we report here that spontaneous and functional reconstitution of PR into "frozen" amphiphilic block copolymer membranes, which have unsurpassed stability as MP-supporting matrices, is achieved *via* the CIDR mechanism. We demonstrated that polymer membranes can be designed to have a balanced local chain-motion freedom and bulk-state membrane stability at the nanoscale, a feature that is critical to harness MP functions in synthetic systems. Even "frozen" polymer membranes can be tuned to bear sufficient conformational freedom that rivals lipid-based biomembranes in supporting MP functions. We also showed that well-defined block copolymer nanomembranes, with their tunable membrane moduli, act as allosteric regulators to support the structural integrity and function of reconstituted PR, likely by modulating its conformational energetics. Given that it is possible to use unidirectionally oriented MPs tethered on a substrate as templates to direct the formation of 2-D supported proteomembrane arrays,[69] and it is also possible to prepare polymersome membranes with removable

hydrophilic mantles[70] to control proteopolymer membrane surface chemistry, we expect that what is learned here may be useful to a subset of other MPs, hence opening a viable approach to the development of MP-based nanotechnologies with optimized stability and performance.

METHODS

Synthesis and Assembly of Proteopolymer Complexes. We used controlled/living free radical polymerization to prepare a series of well-defined amphiphilic triblock copolymers (SI). The polymers were dissolved in dimethylformamide (DMF) and dialyzed against Millipore water using Spectrum MWCO 10−12 kDa dialysis tubes to prepare polymersomes at defined concentrations (∼5−10 mg/mL).

Natural abundance PR was expressed in *E. coli* and purified as described previously.[43] Expression and purification of doubly isotopically labeled ^{13}C,^{15}N-PR for NMR spectroscopy (the wild-type-like mutant C107S/C156S was used, the DNA kindly provided by A. R. Choi and K.-H. Jung, Sogang University, Korea) was performed as described elsewhere,[56] with a single modification. The carbon source was [2-^{13}C]-labeled glycerol (Cambridge Isotope Laboratories) instead of ^{13}C-labeled glucose, to achieve better spectral resolution due to sparse labeling.[71,72]

Proteopolymer complexes were obtained by mixing a prescribed amount of DDM-solubilized PR and amphiphilic block copolymer polymersomes (stoichiometric ratio ∼1:10) in 10 times (in volume) PBS buffer (0.25×, pH = 7.4) with 0.05% DDM. Formation of condensed proteopolymer membrane phase occurred spontaneously without using any external means for detergent removal. The settled proteopolymer complexes were easily separated from the rest of the supernatant and redispersed in a different buffer if needed, for structural and function assays.

Proteoliposome membranes were obtained by reconstituting DDM-solubilized PR into a binary mixture of DMPC/DMPA (9:1 w/w) liposomes *via* Bio-Beads-mediated detergent removal as described earlier,[56] at 2:1 protein/lipid ratio (w/w).

Polymer and Proteopolymer Complexes' Structural Characterization. The chemical structure of synthesized polymers was characterized using a JEOL 500 MHz NMR spectrometer with either $CDCl_3$, DMF-d_7, or dimethyl sulfoxide DMSO-d_6 as a solvent. Their molecular weight was measured by GPC (Viscotek model 270 series platform) with DMF or tetrahydrofuran as the eluent at 55 °C with a flow rate of 1.0 mL/min (columns: ViscoGel I-series G-3000 and G-4000 mixed bed columns: molecular weight range (0−20) × 10^3 and (0−200) × 10^3 g/mol, respectively). The GPC is a triple detector system: a Viscotek differential viscometer/low angle laser light scattering detector (model 270, λ = 670 nm, 3 mW laser, detector angles of 7° and 90°), UV/vis detector (model 3210, λ = 254 nm, tungsten/deuterium lamp), and a refractive index detector model 3580 (10 mV, λ = 660 nm). The instrument was calibrated with polystyrene standards.

DLS of spherical polymersome vesicles was measured by a Malvern Zetasizer Nano ZS90, which automatically sets to accommodate the requirements of high sensitivity by detecting the scattering information at 173° and reports size information with its own software package to fit the photon correlation spectroscopy data. Zeta potentials are measured using the Smoluchowski model.

The glass transition temperature of polymers (T_g) in the solid state was examined with a TA DSC (Q20). Samples (∼20 mg) were placed in an alumina Tzero pan, cooled to −40 °C at a rate of 40 °C/min, equilibrated at −40 °C, and then heated at a rate of 10 °C/min to 150 °C. The cycle was repeated three times under the protection of N_2.

The T_g of polymersome in aqueous solution was measured by a VP-DSC (MicroCal) system. The instrument was equilibrated with a background scan (with water or buffer, the same as that used to prepare poymersomes) overnight before measurement. In a typical run, 0.5 mL of polymersome solution (∼10 mg/mL) was put in a tantalum alloy cell and scanned between 10 and 95 °C at 10 °C/hour. Water or buffer, the same as that used to prepare polymersomes, was used as a reference.

For synchrotron SAXS studies, the proteopolymer complexes were sealed in quartz capillaries (diameter ∼1.5 mm, Hilgenberg GmbH, German) and measured at SSRL (Stanford Synchrotron Radiation Lightsource). Incident synchrotron X-rays from an eight-pole Wiggler was monochromatized (λ = 1.37776 Å) and focused using a cylindrical mirror, and the scattered radiation was collected using a Rayonix MX225-HE detector (pixel size 73.2 μm, 3072 × 3072 array). A typical radiation time at SSRL is 5 s, and each sample was measured six times. No radiation damage was observed for all measurements. The 2-D SAXS powder patterns were integrated using FIT2D (www.esrf.eu/computing/scientific/FIT2D/), and the sample-to-detector distance was calibrated using silver behenate as a standard. The final SAXS data of individual samples were averaged over six different measurements.

The SAXS data were fitted by the nonlinear least-squares method using Igor Pro 6 (WaveMetrics, Lake Oswego, OR, USA). We used a structural model consisting of multilamellar proteopolymer membranes, while testing different forms of 2-D PR lattice models in individual membranes in order to best fit the scattering data. All scattering features were fitted simultaneously to optimize peak positions, scattering amplitudes, and full width at half-maximum. The background scattering was fitted with a power law function, and each scattering peak was fitted with a Gauss function.

For TEM studies, the self-assembled block copolymers or proteopolymer samples (∼5 μL) were put on a 400 mesh ultrathin Type-A grid (Ted Pella) and imaged with a Philips CM200 TEM. An accelerating voltage of 200 kV was used, and the samples were stained with 1% uranyl acetate (UAc) as described previously[44] to enhance contrast.

Raman Spectroscopy. FT-Raman spectroscopy was performed using a Bruker IFS66vs FTIR spectrometer with an FRA106s accessory, with excitation at 1024 nm, at 2 cm^{-1} resolution, using highly concentrated suspensions of proteoliposomes or proteopolymers in 10 mM NaCl, 25 mM CHES, pH 9 buffer at room temperature. Several thousand spectra were averaged to achieve better signal-to-noise ratios. While the same doubly isotopically labeled samples as those used for ssNMR were employed, it should be noted that the retinal is not ^{13}C-labeled, as it was added externally; thus, only ^{15}N isotopic shifts (from lysine Schiff base labeling) can be observed if compared with published Raman spectra of native PR.

Solid-State NMR Spectroscopy. Magic angle spinning ssNMR spectroscopy was performed on an 800 MHz Bruker Avance III NMR spectrometer using a triple resonance $^1H/^{13}C/^{15}N$ E-free magic angle spinning probe, at a spinning rate of 14.3 kHz, and using experimental parameters described earlier.[56,73] A 3−4 mg amount of PR reconstituted in proteoliposome or proteopolymersome complexes was hydrated with a buffer (10 mM NaCl, 25 mM CHES, pH 9), packed into a 3.2 mm rotor, and kept at 5 °C during the experiments (sample temperature). The total experiment time of each 2-D NCA experiment was 4.4 h.

Flash-Photolysis Experiments. For time-resolved laser difference spectroscopy, ∼0.3 mg of PR reconstituted in proteoliposome or proteopolymersome complexes was suspended in the same buffer as used for NMR and Raman measurements. The custom-built flash-photolysis setup was described elsewhere.[74] Sample excitation was provided by the second harmonic of an Nd:YAG laser (Continuum Minilite II) with 7 ns pulses at 532 nm. Several hundred kinetic traces at selected wavelengths were averaged using GAGESCOPE, converted into a quasilogarithmic time-scale, and analyzed by the global exponential fitting using FITEXP.[63] Four exponential components were used in the fittings, and confirmed by F-test to be statistically valid.[59]

Conflict of Interest: The authors declare no competing financial interest.

Acknowledgment. This work was partially supported by NSF through a seed grant from REMRSEC (DMR-0820518), and CBET-1160291 to H.L., as well as by NSERC (Natural Sciences and Engineering Research Council of Canada) grants to V.L. and L.S.B. SAXS experiments were performed at the Stanford Synchrotron Radiation Lightsource, a Directorate of SLAC National Accelerator Laboratory and an Office of Science User Facility operated for the U.S. Department of Energy Office of Science by Stanford University. The authors are grateful to A. R. Choi and K.-H. Jung (Sogang University, Seoul, Korea) for providing the DNA of the wild-type and mutant PR.

Supporting Information Available: Experimental details and additional structural characterizations showing the successful synthesis of a series of well-defined PS-*b*-$(P4MVP)_2$ triblock copolymers *via* controlled/living free radical polymerization methods. This material is available free of charge *via* the Internet at http://pubs.acs.org.

REFERENCES AND NOTES

1. Luckey, M. *Membrane Structural Biology, with Biochemical and Biophysical Foundations*.; Cambridge University Press: New York, 2008; pp 127−159.
2. Midgett, C. R.; Madden, D. R. Breaking the Bottleneck: Eukaryotic Membrane Protein Expression for High-Resolution Structural Studies. *J. Struct. Biol.* **2007**, *160*, 265–274.
3. Schwarz, D.; Dotsch, V.; Bernhard, F. Production of Membrane Proteins Using Cell-Free Expression Systems. *Proteomics* **2008**, *8*, 3933–3946.
4. Mueller, P.; Rudin, D. O.; Tien, H. T.; Wescott, W. C. Reconstitution of Cell Membrane Structure *in Vitro* and Its Transformation into an Excitable System. *Nature* **1962**, *194*, 979–980.
5. Kahya, N. Protein-Protein and Protein-Lipid Interactions in Domain-Assembly: Lessons from Giant Unilamellar Vesicles. *Biochim. Biophys. Acta, Biomembr.* **2010**, *1798*, 1392–1398.
6. Ritchie, T. K.; Grinkova, Y. V.; Bayburt, T. H.; Denisov, I. G.; Zolnerciks, J. K.; Atkins, W. M.; Sligar, S. G. Reconstitution of Membrane Proteins in Phospholipid Bilayer Nanodiscs. *Methods Enzymol.* **2009**, *464*, 211–231.
7. Ranaghan, M. J.; Schwall, C. T.; Alder, N. N.; Birge, R. R. Green Proteorhodopsin Reconstituted into Nanoscale Phospholipid Bilayers (Nanodiscs) as Photoactive Monomers. *J. Am. Chem. Soc.* **2011**, *133*, 18318–18327.
8. Salafsky, J.; Groves, J. T.; Boxer, S. G. Architecture and Function of Membrane Proteins in Planar Supported Bilayers: A Study with Photosynthetic Reaction Centers. *Biochemistry* **1996**, *35*, 14773–14781.
9. Meier, W.; Nardin, C.; Winterhalter, M. Reconstitution of Channel Proteins in (Polymerized) ABA Triblock Copolymer Membranes. *Angew. Chem., Int. Ed.* **2000**, *39*, 4599–4602.
10. Choi, H. J.; Montemagno, C. D. Artificial Organelle: ATP Synthesis from Cellular Mimetic Polymersomes. *Nano Lett.* **2005**, *5*, 2538–2542.
11. Kumar, M.; Grzelakowski, M.; Zilles, J.; Clark, M.; Meier, W. Highly Permeable Polymeric Membranes Based on the Incorporation of the Functional Water Channel Protein Aquaporin Z. *Proc. Natl. Acad. Sci. U.S.A.* **2007**, *104*, 20719–20724.
12. Ihle, S.; Onaca, O.; Rigler, P.; Hauer, B.; Rodriguez-Ropero, F.; Fioroni, M.; Schwaneberg, U. Nanocompartments with a pH Release System Based on an Engineered OmpF Channel Protein. *Soft Matter* **2011**, *7*, 532–539.
13. Zhang, X. Y.; Tanner, P.; Graff, A.; Palivan, C. G.; Meier, W. Mimicking the Cell Membrane with Block Copolymer Membranes. *J. Polym. Sci., Part A: Polym. Chem.* **2012**, *50*, 2293–2318.
14. Ross, E. E.; Rozanski, L. J.; Spratt, T.; Liu, S. C.; O'Brien, D. F.; Saavedra, S. S. Planar Supported Lipid Bilayer Polymers Formed by Vesicle Fusion. 1. Influence of Diene Monomer Structure and Polymerization Method on Film Properties. *Langmuir* **2003**, *19*, 1752–1765.
15. Plant, A. L. Supported Hybrid Bilayer Membranes as Rugged Cell Membrane Mimics. *Langmuir* **1999**, *15*, 5128–5135.
16. Daniel, S.; Albertorio, F.; Cremer, P. S. Making Lipid Membranes Rough, Tough, and Ready to Hit the Road. *MRS Bull.* **2006**, *31*, 536–540.
17. Shim, J. W.; Gu, L. Q. Stochastic Sensing on a Modular Chip Containing a Single-Ion Channel. *Anal. Chem.* **2007**, *79*, 2207–2213.
18. Tanaka, M.; Sackmann, E. Polymer-Supported Membranes as Models of the Cell Surface. *Nature* **2005**, *437*, 656–663.
19. Castellana, E. T.; Cremer, P. S. Solid Supported Lipid Bilayers: From Biophysical Studies to Sensor Design. *Surf. Sci. Rep.* **2006**, *61*, 429–444.
20. Engelman, D. M. Membranes Are More Mosaic Than Fluid. *Nature* **2005**, *438*, 578–580.
21. Kusumi, A.; Nakada, C.; Ritchie, K.; Murase, K.; Suzuki, K.; Murakoshi, H.; Kasai, R. S.; Kondo, J.; Fujiwara, T. Paradigm Shift of the Plasma Membrane Concept from the Two-Dimensional Continuum Fluid to the Partitioned Fluid: High-Speed Single-Molecule Tracking of Membrane Molecules. *Annu. Rev. Biophys. Biomol. Struct.* **2005**, *34*, 351–378.
22. Soubias, O.; Gawrisch, K. Probing Specific Lipid-Protein Interaction by Saturation Transfer Difference NMR Spectroscopy. *J. Am. Chem. Soc.* **2005**, *127*, 13110–13111.
23. Alvis, S. J.; Williamson, I. M.; East, J. M.; Lee, A. G. Interactions of Anionic Phospholipids and Phosphatidylethanolamine with the Potassium Channel KcsA. *Biophys. J.* **2003**, *85*, 3828–3838.
24. Opekarova, M.; Tanner, W. Specific Lipid Requirements of Membrane Proteins - A Putative Bottleneck in Heterologous Expression. *Biochim. Biophys. Acta, Biomembr.* **2003**, *1610*, 11–22.
25. Valiyaveetil, F. I.; Zhou, Y. F.; Mackinnon, R. Lipids in the Structure, Folding, and Function of the KcsA K^+ Channel. *Biochemistry* **2002**, *41*, 10771–10777.
26. Mitchell, D. C.; Lawrence, J. T. R.; Litman, B. J. Primary Alcohols Modulate the Activation of the G Protein-Coupled Receptor Rhodopsin by a Lipid-Mediated Mechanism. *J. Biol. Chem.* **1996**, *271*, 19033–19036.
27. Cantor, R. S. Lipid Composition and the Lateral Pressure Profile in Bilayers. *Biophys. J.* **1999**, *76*, 2625–2639.
28. Brown, M. F. Curvature Forces in Membrane Lipid-Protein Interactions. *Biochemistry* **2012**, *51*, 9782–9795.
29. Andersen, O. S.; Koeppe, R. E. Bilayer Thickness and Membrane Protein Function: An Energetic Perspective. *Annu. Rev. Biophys. Biomol. Struct.* **2007**, *36*, 107–130.
30. Phillips, R.; Ursell, T.; Wiggins, P.; Sens, P. Emerging Roles for Lipids in Shaping Membrane-Protein Function. *Nature* **2009**, *459*, 379–385.
31. Marsh, D.; Horvath, L. I. Structure, Dynamics and Composition of the Lipid-Protein Interface. Perspectives from Spin-Labelling. *Biochim. Biophys. Acta, Rev. Biomembr.* **1998**, *1376*, 267–296.
32. Lee, A. G. Lipid-Protein Interactions in Biological Membranes: A Structural Perspective. *Biochim. Biophys. Acta, Biomembr.* **2003**, *1612*, 1–40.
33. Soubias, O.; Gawrisch, K. The Role of the Lipid Matrix for Structure and Function of the GPCR Rhodopsin. *Biochim. Biophys. Acta, Biomembr.* **2012**, *1818*, 234–240.
34. Lee, A. G. Biological Membranes: The Importance of Molecular Detail. *Trends Biochem. Sci.* **2011**, *36*, 493–500.
35. Prive, G. G. Detergents for the Stabilization and Crystallization of Membrane Proteins. *Methods* **2007**, *41*, 388–397.
36. Eytan, G. D. Use of Liposomes for Reconstitution of Biological Functions. *Biochim. Biophys. Acta* **1982**, *694*, 185–202.
37. Rigaud, J. L.; Levy, D. Reconstitution of Membrane Proteins into Liposomes. *Methods Enzymol.* **2003**, *372*, 65–86.
38. Rigaud, J. L.; Paternostre, M. T.; Bluzat, A. Mechanisms of Membrane-Protein Insertion into Liposomes during Reconstitution Procedures Involving the Use of Detergents 0.2. Incorporation of the Light-Driven Proton Pump Bacteriorhodopsin. *Biochemistry* **1988**, *27*, 2677–2688.

39. Casey, R. P. Membrane Reconstitution of the Energy-Conserving Enzymes of Oxidative Phosphorylation. *Biochim. Biophys. Acta* **1984**, *768*, 319–347.
40. Ollivon, M.; Lesieur, S.; Grabielle-Madelmont, C.; Paternostre, M. Vesicle Reconstitution from Lipid-Detergent Mixed Micelles. *Biochim. Biophys. Acta, Biomembr.* **2000**, *1508*, 34–50.
41. Beja, O.; Aravind, L.; Koonin, E. V.; Suzuki, M. T.; Hadd, A.; Nguyen, L. P.; Jovanovich, S. B.; Gates, C. M.; Feldman, R. A.; Spudich, J. L.; *et al*. Bacterial Rhodopsin: Evidence for a New Type of Phototrophy in the Sea. *Science* **2000**, *289*, 1902–1906.
42. Beja, O.; Spudich, E. N.; Spudich, J. L.; Leclerc, M.; DeLong, E. F. Proteorhodopsin Phototrophy in the Ocean. *Nature* **2001**, *411*, 786–789.
43. Liang, H. J.; Whited, G.; Nguyen, C.; Okerlund, A.; Stucky, G. D. Inherently Tunable Electrostatic Assembly of Membrane Proteins. *Nano Lett.* **2008**, *8*, 333–339.
44. Liang, H. J.; Whited, G.; Nguyen, C.; Stucky, G. D. The Directed Cooperative Assembly of Proteorhodopsin into 2D and 3D Polarized Arrays. *Proc. Natl. Acad. Sci. U.S.A.* **2007**, *104*, 8212–8217.
45. Hua, D. B.; Kuang, L. J.; Liang, H. J. Self-Directed Reconstitution of Proteorhodopsin with Amphiphilic Block Copolymers Induces the Formation of Hierarchically Ordered Proteopolymer Membrane Arrays. *J. Am. Chem. Soc.* **2011**, *133*, 2354–2357.
46. Kuang, L. J.; Olsen, T. L.; Lin, S.; Flores, M.; Jiang, Y. J.; Zheng, W.; Williams, J. C.; Allen, J. P.; Liang, H. J. Interface for Light-Driven Electron Transfer by Photosynthetic Complexes across Block Copolymer Membranes. Under review by *J. Phys. Chem. Lett.* **2013**.
47. Moad, G.; Rizzardo, E.; Thang, S. H. Living Radical Polymerization by the RAFT Process. *Aust. J. Chem.* **2005**, *58*, 379–410.
48. Patten, T. E.; Matyjaszewski, K. Atom Transfer Radical Polymerization and the Synthesis of Polymeric Materials. *Adv. Mater.* **1998**, *10*, 901–915.
49. Lai, J. T.; Filla, D.; Shea, R. Functional Polymers from Novel Carboxyl-Terminated Trithiocarbonates as Highly Efficient RAFT Agents. *Macromolecules* **2002**, *35*, 6754–6756.
50. Bermudez, H.; Brannan, A. K.; Hammer, D. A.; Bates, F. S.; Discher, D. E. Molecular Weight Dependence of Polymersome Membrane Structure, Elasticity, and Stability. *Macromolecules* **2002**, *35*, 8203–8208.
51. Discher, D. E.; Eisenberg, A. Polymer Vesicles. *Science* **2002**, *297*, 967–973.
52. Rubinstein, M.; Colby, R. H. *Polymer Physics*; Oxford University Press Inc.: New York, 2003; p 53.
53. Pata, V.; Dan, N. The Effect of Chain Length on Protein Solubilization in Polymer-Based Vesicles (Polymersomes). *Biophys. J.* **2003**, *85*, 2111–2118.
54. Srinivas, G.; Discher, D. E.; Klein, M. L. Key Roles for Chain Flexibility in Block Copolymer Membranes That Contain Pores or Make Tubes. *Nano Lett.* **2005**, *5*, 2343–2349.
55. Klyszejko, A. L.; Shastri, S.; Mari, S. A.; Grubmuller, H.; Muller, D. J.; Glaubitz, C. Folding and Assembly of Proteorhodopsin. *J. Mol. Biol.* **2008**, *376*, 35–41.
56. Shi, L. C.; Ahmed, M. A. M.; Zhang, W. R.; Whited, G.; Brown, L. S.; Ladizhansky, V. Three-Dimensional Solid-State NMR Study of a Seven-Helical Integral Membrane Proton Pump-Structural Insights. *J. Mol. Biol.* **2009**, *386*, 1078–1093.
57. Shi, L. C.; Lake, E. M. R.; Ahmed, M. A. M.; Brown, L. S.; Ladizhansky, V. Solid-State NMR Study of Proteorhodopsin in the Lipid Environment: Secondary Structure and Dynamics. *Biochim. Biophys. Acta, Biomembr.* **2009**, *1788*, 2563–2574.
58. Wishart, D. S.; Sykes, B. D.; Richards, F. M. The Chemical-Shift Index - A Fast and Simple Method for the Assignment of Protein Secondary Structure through NMR-Spectroscopy. *Biochemistry* **1992**, *31*, 1647–1651.
59. Dioumaev, A. K.; Brown, L. S.; Shih, J.; Spudich, E. N.; Spudich, J. L.; Lanyi, J. K. Proton Transfers in the Photochemical Reaction Cycle of Proteorhodopsin. *Biochemistry* **2002**, *41*, 5348–5358.
60. Friedrich, T.; Geibel, S.; Kalmbach, R.; Chizhov, I.; Ataka, K.; Heberle, J.; Engelhard, M.; Bamberg, E. Proteorhodopsin Is a Light-Driven Proton Pump with Variable Vectoriality. *J. Mol. Biol.* **2002**, *321*, 821–838.
61. Varo, G.; Brown, L. S.; Lakatos, M.; Lanyi, J. K. Characterization of the Photochemical Reaction Cycle of Proteorhodopsin. *Biophys. J.* **2003**, *84*, 1202–1207.
62. Fernandes, D. Lipid Modulation of Dynamics of a Seven-Helical Transmembrane Protein, Proteorhodopsin. M.Sc. Thesis, University of Guelph, Ontario, Canada, 2013; pp 37−48.
63. Dioumaev, A. K. Evaluation of Intrinsic Chemical Kinetics and Transient Product Spectra from Time-Resolved Spectroscopic Data. *Biophys. Chem.* **1997**, *67*, 1–25.
64. Andersson, M.; Malmerberg, E.; Westenhoff, S.; Katona, G.; Cammarata, M.; Wohri, A. B.; Johansson, L. C.; Ewald, F.; Eklund, M.; Wulff, M.; *et al*. Structural Dynamics of Light-Driven Proton Pumps. *Structure* **2009**, *17*, 1265–1275.
65. Israelachvili, J. N. *Intermolecular and Surface Forces*, 2nd ed.; Academic Press: London, 1991; p 377.
66. Marsh, D.; Bartucci, R.; Sportelli, L. Lipid Membranes with Grafted Polymers: Physicochemical Aspects. *Biochim. Biophys. Acta, Biomembr.* **2003**, *1615*, 33–59.
67. Evans, E. Bending Resistance and Chemically Induced Moments in Membrane Bilayers. *Biophys. J.* **1974**, *14*, 923–931.
68. Helfrich, W. Effect of Thermal Undulations on the Rigidity of Fluid Membranes and Interfaces. *J. Phys. (Paris)* **1985**, *46*, 1263–1268.
69. Ataka, K.; Giess, F.; Knoll, W.; Naumann, R.; Haber-Pohlmeier, S.; Richter, B.; Heberle, J. Oriented Attachment and Membrane Reconstitution of His-Tagged Cytochrome c Oxidase to a Gold Electrode: *in situ* Monitoring by Surface-Enhanced Infrared Absorption Spectroscopy. *J. Am. Chem. Soc.* **2004**, *126*, 16199–16206.
70. Brinkhuis, R. P.; Visser, T. R.; Rutjes, F.; van Hest, J. C. M. Shedding the Hydrophilic Mantle of Polymersomes. *Polym. Chem.* **2011**, *2*, 550–552.
71. Higman, V. A.; Flinders, J.; Hiller, M.; Jehle, S.; Markovic, S.; Fiedler, S.; van Rossum, B. J.; Oschkinat, H. Assigning Large Proteins in the Solid State: A MAS NMR Resonance Assignment Strategy Using Selectively and Extensively C-13-Labelled Proteins. *J. Biomol. NMR* **2009**, *44*, 245–260.
72. Castellani, F.; van Rossum, B.; Diehl, A.; Schubert, M.; Rehbein, K.; Oschkinat, H. Structure of a Protein Determined by Solid-State Magic-Angle-Spinning NMR Spectroscopy. *Nature* **2002**, *420*, 98–102.
73. Emami, S.; Fan, Y.; Munro, R.; Ladizhansky, V.; Brown, L. S. Yeast-Expressed Human Membrane Protein Aquaporin-1 Yields Excellent Resolution of Solid-State MAS NMR Spectra. *J. Biomol. NMR* **2013**, *55*, 147–155.
74. Waschuk, S. A.; Bezerra, A. G.; Shi, L.; Brown, L. S. Leptosphaeria Rhodopsin: Bacteriorhodopsin-Like Proton Pump from a Eukaryote. *Proc. Natl. Acad. Sci. U.S.A.* **2005**, *102*, 6879–6883.